Summer-Winter Contrast in the Response of Precipitation Extremes to Climate Change Over Northern Hemisphere Land

Andrew I. L. Williams[1] [ID] **and Paul A. O'Gorman[2]** [ID]

[1]Atmospheric, Oceanic and Planetary Physics, Department of Physics, University of Oxford, Oxford, UK, [2]Department of Earth, Atmospheric and Planetary Sciences, Massachusetts Institute of Technology, Cambridge, MA, USA

Abstract Climate models project a distinct seasonality to future changes in daily extreme precipitation. In particular, models project that over land in the extratropical Northern Hemisphere the summer response is substantially weaker than the winter response in percentage terms. Here we decompose the projected response into thermodynamic and dynamic contributions and show that the seasonal contrast arises due to a negative dynamic contribution in northern summer, and a positive dynamic contribution and an anomalously strong thermodynamic contribution in northern winter. The negative dynamic contribution in northern summer is due to weakened ascent and is strongly correlated with decreases in mean near-surface relative humidity. Finally, we show that the summer-winter contrast is also evident in observed trends of daily precipitation extremes in northern midlatitudes, which provides support for the contrast found in climate-model simulations.

Plain Language Summary Extreme rainfall is a highly impactful aspect of the water cycle, and it is now well-established that global warming tends to increase the severity of extreme rainfall events. However, while this increase holds robustly on global scales, there is significant uncertainty associated with understanding the response of extreme rainfall to warming in different regions of the world and in different seasons. Here we focus on understanding changes in extreme rainfall in summer and winter over Northern Hemisphere extratropical land. We find that global warming has a contrasting impact on extreme rainfall over this region depending on the season considered. In winter, there are large increases in extreme rainfall with warming relative to the climatology, whereas in summer the changes are much weaker. We use a simple, physics-based approach to decompose these changes into contributions from changes in temperature and changes in ascent. Our results show that the contrasting seasonal response over this region is mostly due to decreases in extreme ascent with warming in summer, and that the "summer-winter" contrast is already present in observed changes of extreme rainfall since the mid-20th century.

1. Introduction

The impacts of extreme precipitation are felt acutely across the world with consequences ranging from floods and landslides (Kirschbaum et al., 2012) to changes in ecosystems (Knapp et al., 2008). Additionally, it is now well-understood that extreme precipitation events intensify overall on a global scale in response to global warming (Kharin et al., 2013; O'Gorman, 2015; Wehner et al., 2020). On regional scales however, the response of precipitation extremes to warming is uncertain, with some regions projected to experience changes in precipitation extremes which are much higher or lower than the global-mean intensification (Pfahl et al., 2017). Put together, this makes regional changes in extreme precipitation potentially one of the most impactful consequences of global warming. Thus, understanding historical and future changes in regional extreme precipitation important not only from a scientific perspective, but also for understanding the unequal impacts of climate change (Diffenbaugh & Burke, 2019). In addition, considering precipitation extremes in different seasons helps to clarify physical drivers and can also be important for impacts.

To understand projections of changes in precipitation extremes it is useful to decompose the changes into contributions from different physical drivers. One such approach is to use the simple, physical scaling developed by O'Gorman and Schneider (2009a) which relates the intensity of precipitation extremes, P_e, to the pressure vertical velocity (ω_e) and the vertical derivative of saturation specific humidity with respect to pressure assuming a moist adiabatic lapse rate $\left(\frac{dq_s}{dp} \big|_{\theta*} \right)$,

$$P_e \sim -\left\{ \omega_e \frac{dq_s}{dp} \bigg|_{\theta*} \right\}, \tag{1}$$

where $\{\cdot\}$ denotes a mass-weighted vertical integral over the troposphere, ω_e is evaluated on the day of the extreme event, and $\frac{dq_s}{dp}|_{\theta^*}$ is evaluated using the temperature T_e on the day of the extreme event. Thus, when considering a change in precipitation extremes due to global warming, δP_e, we can decompose the change into a thermodynamic contribution associated with changes in T_e and a dynamic contribution associated with changes in extreme ascent ω_e,

$$\delta P_e \approx \delta P_{\text{thermodynamic}} + \delta P_{\text{dynamic}}. \tag{2}$$

Pfahl et al. (2017) recently showed that Equation 1 successfully captures the present-day and future changes of precipitation extremes in simulations from the Coupled Model Intercomparison Project Phase 5, CMIP5, (Taylor et al., 2012) and thus is a good proxy for understanding and decomposing these future changes (Figure S1 in Supporting Information S1). Pfahl et al. (2017) used Equation 1 to decompose future regional changes in annual and seasonal maximum daily precipitation (hereafter, Rx1day) in the CMIP5 simulations into thermodynamic and dynamic contributions. The thermodynamic contribution is positive and relatively spatially uniform, whereas the dynamic contribution varies strongly between regions and seasons and can either locally amplify or counteract the increases from the thermodynamic contribution.

The results of Pfahl et al. (2017) show a pronounced "summer-winter" contrast in the response of seasonal Rx1day. The fraction of Northern Hemisphere (NH) extratropical land experiencing robust increases is relatively small in June-July-August (JJA), due to a negative dynamic contribution over land, particularly over Europe and North America. Similar results were found by Tandon et al. (2018) for the CanESM2 large ensemble. By contrast, Pfahl et al. (2017) found a strong response of precipitation extremes in the NH extratropics for December-January-February (DJF), and climate change was found to induce a shift in precipitation extremes toward the cold season in this region. Marelle et al. (2018) also found a shift toward the cold season for many regions in both CMIP5 models and regional models from the Coordinated Regional Downscaling Experiment (CORDEX). Furthermore, although climate models exhibit regional biases in precipitation extremes (Pfahl et al., 2017), Marelle et al. (2018) found that the CMIP5 and CORDEX models reproduce most aspects of the seasonality of precipitation extremes in the current climate when compared to gridded observations, which increases confidence in their future projections for changes in seasonality.

High-resolution, regional models have also shown a weaker response of precipitation extremes to climate change in JJA than DJF in Europe (Wood & Ludwig, 2020). This summer-winter contrast was also found in convection-permitting simulations of the Mediterranean (Pichelli et al., 2021) and the Contiguous United States (Prein et al., 2017), which is notable since convection-permitting simulations are better able to represent short-duration precipitation extremes (Prein et al., 2015). Precipitation extremes in JJA are known to be sensitive to how convection is represented (Ban et al., 2015; Chan et al., 2014; Kooperman et al., 2014; Prein et al., 2015), and caution is needed for projections in regions and seasons with significant mesoscale convective activity, particularly for sub-daily extremes. This emphasizes the importance of seeking observational evidence and robust physical mechanisms that may support projected seasonal changes in precipitation extremes.

Here, we focus on the summer-winter contrast in the fractional response of daily precipitation extremes to climate warming in the NH in CMIP5 models and gridded observations. We begin by describing the model output and observational data and the methods of analysis (Section 2). We then show that the JJA-DJF contrast is primarily due to differences in the dynamic contribution between JJA and DJF, but that differences in the thermodynamic contribution also play a role, particularly at high latitudes (Section 3). We further show that the negative dynamic contribution in JJA is strongly correlated in terms of model scatter and spatial pattern to decreases in mean near-surface relative humidity over land and explore possible physical mechanisms for this negative dynamic contribution (Section 4). Finally, we demonstrate that the summer-winter contrast is also evident in gridded observational datasets and CMIP5 simulations over the historical period (Section 5), before giving our conclusions (Section 6).

2. Methods

We analyze changes over 1950–2100 under the historical and RCP8.5 scenarios for CMIP5. All models are used that provide the required data (listed in Text S1 in Supporting Information S1). The scaling and decomposition based on Equation 1 is taken from Pfahl et al. (2017), and further details can be found there, but we repeat the key
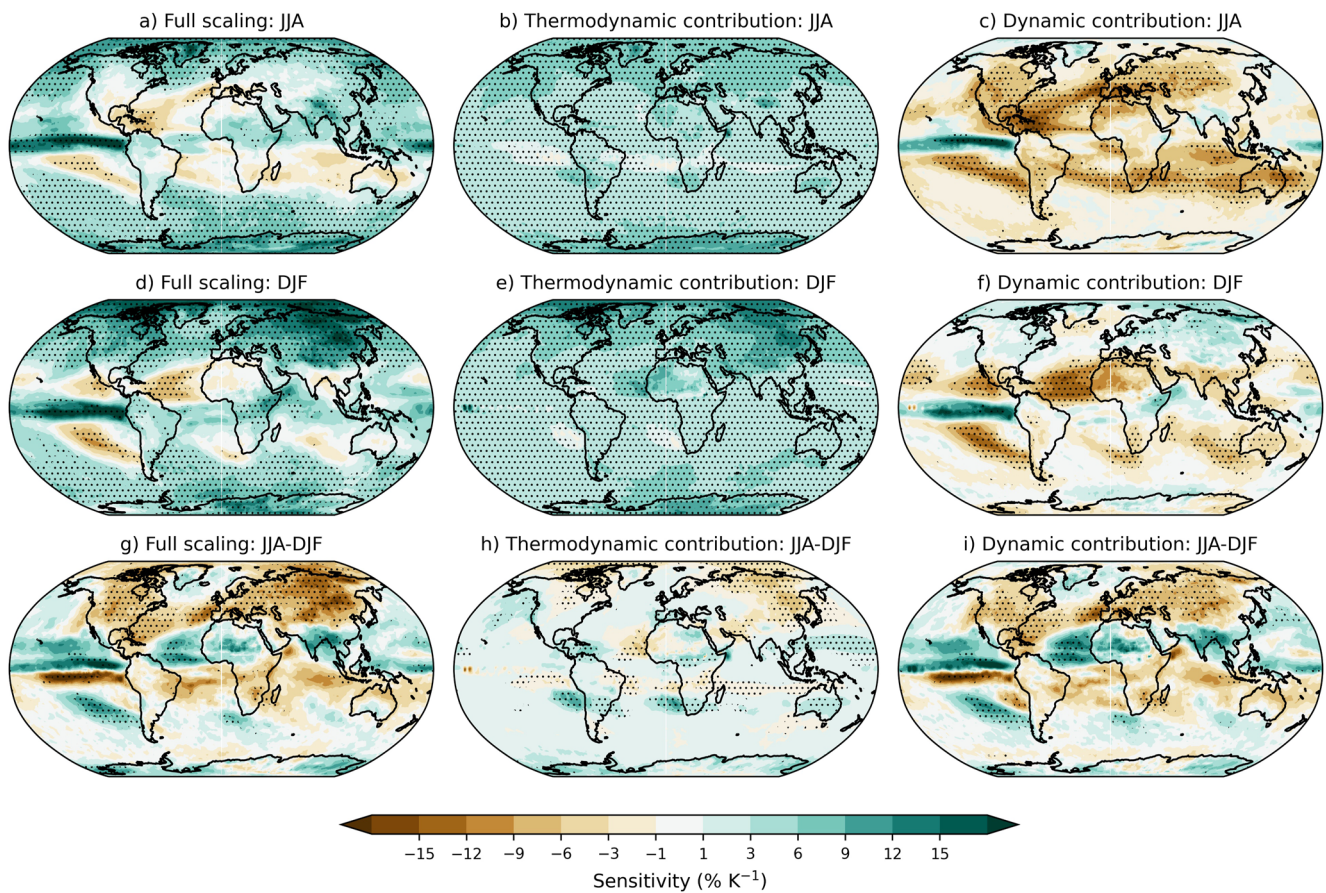
Figure 1. Multi-model mean Rx1day sensitivity over 1950–2100 according to the scaling Equation 1 (a,d, and g) and decomposition into (b,e, and h) thermodynamic and (c,f, and i) dynamic contributions for panels (a–c) June-July-August (JJA), (d–f) December-January-February (DJF) and (e–i) JJA minus DJF, the summer-winter contrast. Stippling indicates where at least 90% of the models agree on the sign of the change.

points of the calculation here. We chose not to repeat their calculations with CMIP6 output because there is little improvement in the simulation of daily precipitation extremes between CMIP5 and CMIP6 (Wehner et al., 2020).

Daily surface precipitation was used to calculate the maximum daily precipitation amount (Rx1day) for JJA and DJF in each year. Daily-mean temperature and vertical pressure velocity on all available pressure levels at the location and day of each daily-maximum precipitation event (T_e and ω_e, respectively) were then used to calculate the full extreme precipitation scaling following Equation 1 by performing a vertical integral over all tropospheric levels with ascent ($\omega_e < 0$). To calculate the thermodynamic contribution, this analysis is repeated but with ω_e replaced with its average over all years from 1950 to 2100.

To calculate the sensitivity to climate change, we first normalize Rx1day and the full and thermodynamic scalings by dividing by their average over the historical period (1950–2000). We then calculate the dynamic contribution as the difference between the full and thermodynamic scaling. This approach to calculating the dynamic contribution differs slightly from Pfahl et al. (2017), but yields similar results (e.g., compare our Figure 1c with their Figure S8d in Supporting Information S1). We then regress these normalized time series against global- and annual-mean surface temperature anomalies over 1950–2000 using the Theil-Sen estimator to produce sensitivities in units of (% K^{-1}). The Theil-Sen estimator is a non-parametric estimator which operates by choosing the median of the slopes of all lines through pairs of points and is less sensitive to outliers than ordinary least-squares regression. This regression approach has been shown to provide more robust results compared to taking differences in multi-decadal means (Fischer et al., 2014). When presenting results for the seasonal contrast (JJA-DJF), the sensitivities are calculated by differencing the normalized JJA and DJF time series in each grid box, before regressing this "difference" time series against global-mean surface temperature anomalies for each model. Using a normalization over a reference period can sometimes produce statistical biases for changes in precipitation

extremes (Donat et al., 2016; Sippel et al., 2017), but our results remain largely unchanged when using the full 1950–2100 period for normalization (Figure S2 in Supporting Information S1).

All analysis is performed on each model's native grid, and then the sensitivities are re-gridded to a uniform $1° \times 1°$ grid before calculating multi-model statistics and zonal means. Pfahl et al. (2017) noted previously that some models produce very low seasonal Rx1day at some grid points in the subtropics, which creates anomalously large extreme precipitation sensitivities. Thus, when calculating multi-model or zonal means we exclude grid boxes from models where the average seasonal Rx1day over the historical period is less than 0.5 mm day^{-1}. Additionally, we found that the CMCC-CMS model produced unrealistically large changes in the thermodynamic contribution over Pakistan and Afghanistan, and so for this model we exclude the region from 29.5° to 32.5° latitude and 60°–68° longitude.

We also analyze changes in seasonal Rx1day over the historical period over land in observations and compare them to the same period in the CMIP5 simulations (combining the historical and RCP8.5 simulations). We analyze the "extended" NH summer (MJJAS) and winter (NDJFM) seasons (as opposed to JJA and DJF) to improve the signal-to-noise ratio and use data from 1950 to 2017, with the time-period chosen for maximum overlap with the CMIP5 data. For Rx1day observations, we focus on the HadEX3 gridded data set (Dunn et al., 2020) which has a spatial resolution of $1.25° \times 1.875°$, but we also show results for the GHCNDEX observational data set over 1952–2018 (Donat et al., 2013) which has a resolution of $2.5° \times 2.5°$ in the supplement as a point of comparison. To calculate annual- and global-mean surface temperatures (including land and ocean) from observations, we use the NOAA Merged Land-Ocean Surface Temperature Analysis (Vose et al., 2012).

Sensitivities in % K^{-1} for the observations are calculated at each gridbox as described earlier but requiring at least 45 years of data at that grid box and normalizing by an average over all the years used. When analyzing the summer-winter contrast (here, MJJAS-NDJFM) we require each grid box to have 45 years of data for both seasons in each year, and we normalize each time series separately before differencing and then performing the regression. CMIP5 data are subsampled to the observations in both space and time. To reduce the influence of unforced variability and outliers, we then aggregate the sensitivities into 5° latitude bands and calculate the median sensitivity across each latitude band. We use bootstrapping to estimate the uncertainty due to inter-annual variability and the non-uniform spatial coverage of the observations. To do this we calculate 10,000 bootstrap samples per latitude band, where each sample involves a random choice of both the years used for each grid box to calculate the regression, and a random choice of the grid boxes used to calculate the median sensitivity across the latitude band. We then calculate the median sensitivity for each bootstrap sample, and then the 90% confidence interval across samples for each latitude band. Our conclusions are largely insensitive to the size of the latitude bands and the number of bootstrap samples used, except in the tropics where larger latitude bands can obscure seasonal migrations of the ITCZ.

3. Summer-Winter Contrast in CMIP5

Figure 1 shows the multi-model mean patterns of seasonal Rx1day sensitivity based on the scaling Equation 1 and its decomposition into thermodynamic and dynamic contributions for JJA, DJF and JJA-DJF. As found in previous studies, the thermodynamic contribution is relatively uniform with robust agreement on the sign and the magnitude in both seasons. In stark contrast, the dynamic contribution exhibits strong regional and seasonal variations.

The NH extratropics show a strongly negative JJA-DJF contrast especially over land (Figure 1g). Over this region, the DJF response (Figure 1d) is amplified by a positive contribution from the dynamics (Figure 1f) and a relatively strong thermodynamic contribution particularly at high latitudes (Figure 1e). On the other hand, the response during JJA is "muted", with much less multi-model agreement and with some regions (particularly Europe and the continental United States) exhibiting close to no change or even negative responses of extreme precipitation to warming (Figure 1a). This weak JJA response arises predominantly due to the strongly negative dynamic contribution (Figure 1c) which cancels out the robust, positive increase due to the thermodynamic contribution (Figure 1b). The negative dynamic contribution in JJA is particularly strong over land and parts of the subtropical Atlantic. A land-ocean contrast in the dynamic contribution in JJA is apparent when examining anomalies from the zonal-mean (Figure S3 in Supporting Information S1), which show that the negative dynamic contribution extends further poleward over NH land as compared to ocean. The combination of the very weak response in JJA
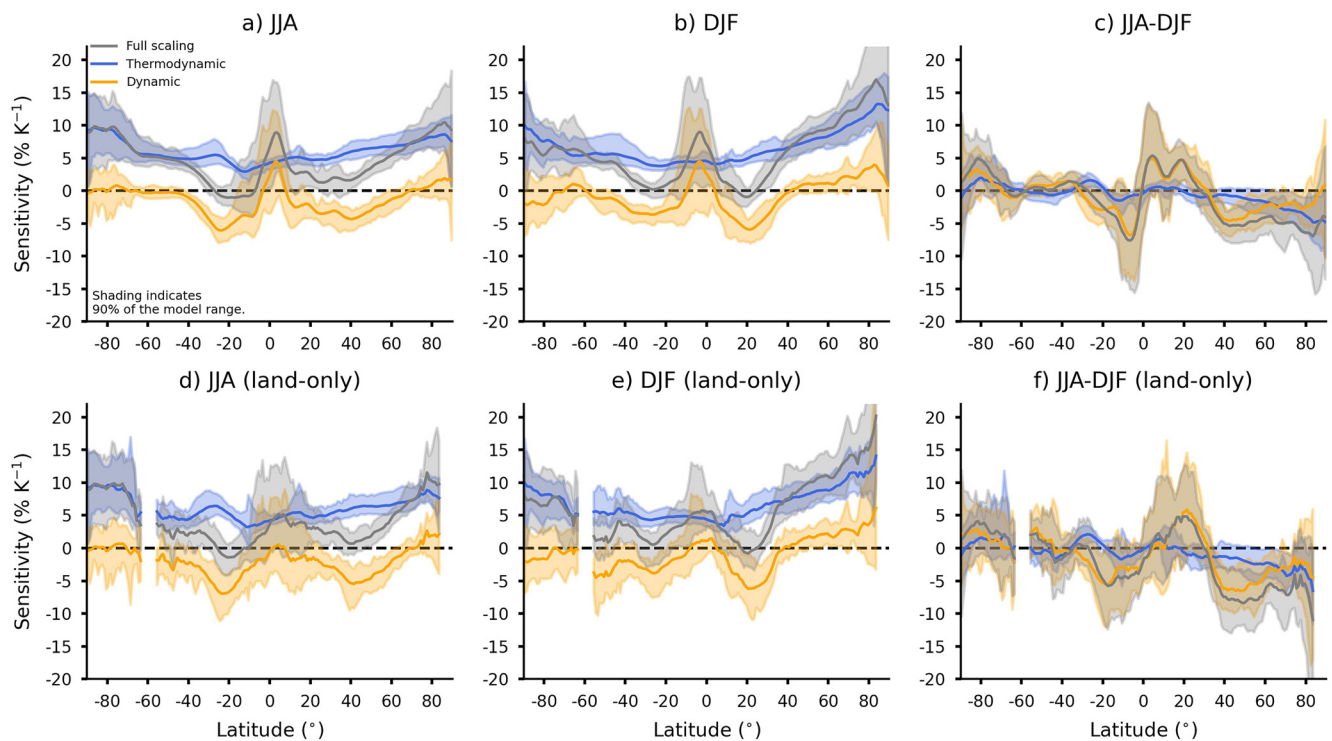
Figure 2. Zonal-mean of the Rx1day sensitivity over 1950–2100 according to the scaling and its decomposition into thermodynamic and dynamic contributions for (a) June-July-August (JJA), (b) December-January-February (DJF) and (c) JJA-DJF. Lines indicate multi-model means and shading shows the 90% model range. Panels (d,e, and f) show the same results but for over land only.

and the amplified response in DJF leads to the strong JJA-DJF difference in the response, particularly over NH midlatitude land. The dynamic contribution is responsible for most of the JJA-DJF difference, as illustrated by the similarity between Figures 1g and 1i, but seasonal differences in the thermodynamic contribution also play a role (Figure 1h).

We next examine zonal-mean changes in the scaling decomposition over both land and ocean and over land only (Figure 2). The thermodynamic contribution is larger at higher latitudes (e.g., Figures 2b and 2e) and is partly responsible for the JJA-DJF contrast at NH middle and high latitudes (Figures 2c and 2f), implying a stronger thermodynamic contribution in DJF than JJA. A stronger thermodynamic contribution is expected for the lower temperatures in winter and at higher latitudes because percentage increases in $\frac{dq_s}{dp}|_{\theta^*}$ with increasing temperature are larger at lower temperatures (O'Gorman & Schneider, 2009a). It could also be argued that Arctic amplification of surface warming also plays a role, and indeed the JJA-DJF contrast in the NH thermodynamic contribution is negligible when we regress against zonal-mean temperature (Figure S4 in Supporting Information S1). However, the stronger thermodynamic contribution at higher (and colder) latitudes is also found to occur even when a globally uniform surface warming is imposed (O'Gorman et al., 2021) suggesting that it is not tied to Arctic amplification. Additionally, previous studies have found there is less warming of T_e than mean temperature at middle and high latitudes (e.g., Figure S5 of O'Gorman and Schneider (2009a) or Figure 8c of O'Gorman and Schneider (2009b)) which suggests that normalizing by the local changes in zonal-mean temperature gives too much emphasis to Arctic amplification.

In the tropics, the zonal-mean results in Figure 2 are consistent with amplification of precipitation extremes along the ITCZ region, which moves seasonally. This leads to a southward shift in precipitation extremes when considering the summer-winter contrast (Figures 2c and 2f) because the ITCZ occurs further south in DJF than in JJA. These shifts are driven by the dynamic contribution as demonstrated by the similarity between the changes in the full scaling and the dynamic contribution in the tropics (gray and orange lines in Figures 2c and 2f).

We have presented results in terms of percentage changes in (% K^{-1}) as opposed to absolute changes (mm day^{-1} K^{-1}) because it is useful to consider the change in each season relative to what is expected for that season

and because previous studies have also focused on percentage changes which are easier to relate to physical processes. Absolute changes also show a seasonal contrast for much of NH midlatitude land but not for some parts of Asia (Figure S5g in Supporting Information S1) or for zonal-mean quantities (Figure S6f in Supporting Information S1), because the thermodynamic contribution offsets the dynamic contribution when considering absolute changes. Thus, one additional advantage of considering percentage changes is that it provides a strong zonal-mean signal to look for in the observational record (Section 5).

4. Physical Mechanisms of the Negative Dynamic Contribution in JJA

Dynamic weakening of precipitation extremes during JJA is a large contributor to the JJA-DJF contrast in the extratropical NH, particularly over land (Figures 1c and 2d). Physically then, what mechanisms could be responsible for this dynamic weakening? Tandon et al. (2018) tackled this question using a three-term approximation of the QG-ω equation and found the weakening of extreme ascent was related to increases in the horizontal length scale of extreme ascent. However, Li and O'Gorman (2020) numerically inverted the QG-ω equation in extreme precipitation events and found that changes in eddy length were less important when all terms were retained in the QG-ω equation, although they did not separately analyze extremes in JJA. Changes in moist static stability, σ_m, have also been found to be important in previous studies (Li & O'Gorman, 2020; Tandon et al., 2018), with an increase in σ_m associated with a weakening of ascent. Here, we calculate changes in moist static stability on the days of the extreme events following previous work (Text S2 in Supporting Information S1) and find that the changes in moist static stability are mostly consistent with the spatial pattern of the JJA dynamic contribution (Figure S7 in Supporting Information S1), but they fail to capture the inter-model spread in projections over NH land (Figure S8 in Supporting Information S1).

The fact that precipitation extremes in JJA over NH extratropical land are convective in nature motivates us to investigate an mechanism for the dynamic contribution in terms of changes in low-level relative humidity which would affect the environment for convection and the associated convective heating that amplifies large-scale ascent. Decreases in near-surface relative humidity (RH$_{2m}$) over land are expected with global-warming because of the land-ocean warming contrast (Byrne & O'Gorman, 2016; Byrne & O'Gorman, 2018) and decreases in stomatal conductance (Berg et al., 2016; Cao et al., 2010). Furthermore, previous work has shown that decreases in relative humidity cause an increase in convective inhibition (CIN) that is particularly large over NH land in JJA (Chen et al., 2020).

In Figure 3 we compare the sensitivities of seasonal-mean RH$_{2m}$ and the dynamic contribution to precipitation extremes during JJA for climate change over 1950–2100. The sensitivity of RH$_{2m}$ is defined using regression analogously to the sensitivity of precipitation extremes and normalized by the 1950–2000 mean. There is strong agreement between the spatial pattern of the change in RH$_{2m}$ and the dynamic contribution (Figures 3a and 3b), with the models agreeing robustly on strong decreases in relative humidity and a negative dynamic contribution over similar regions of the globe. Furthermore, Figure 3c shows that models with a stronger decrease in JJA RH$_{2m}$ also tend to have a stronger negative dynamic contribution when averaged over NH midlatitude land. The link between the dynamic contribution and RH$_{2m}$ is not as strong in individual model runs (Figures S9 and S10 in Supporting Information S1), potentially due to unforced variability in precipitation extremes and other mechanisms which act to change ω_e in precipitation extremes but are not robust across models. Changes in RH$_{2m}$ on the day of the event are weaker but are nonetheless strongly correlated with the dynamic contribution (Figure S11 in Supporting Information S1).

The details of the mechanism by which decreases in relative humidity inhibit convective heating in extreme precipitation events requires further study, ideally with a cloud-resolving model (Muller et al., 2011; Singh & O'Gorman, 2013). One possibility is through increases in CIN, and we find that seasonal-mean CIN increases are correlated with the dynamic contribution for both the spatial pattern and inter-model scatter (Text S3 and Figure S12 in Supporting Information S1) (Lepore et al., 2021). However, while CIN on the day of the extreme precipitation event (CIN^e) also increases, these changes are not strongly correlated with the dynamic contribution in terms of inter-model scatter (see Figures S13 and S14 and discussion in Text S3 in Supporting Information S1). Thus, low-level relative humidity decreases may be inhibiting convection, but CIN on the day of the event does not clearly capture this effect. Relative humidity higher up in the troposphere on the day of the event also decreases
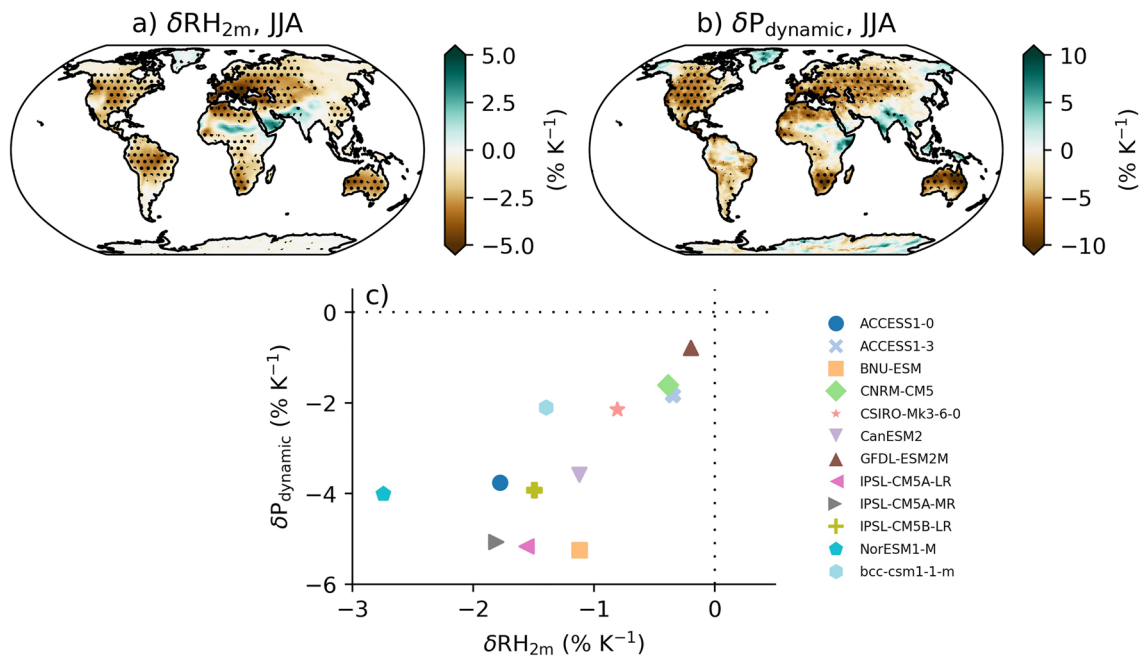
Figure 3. Sensitivity for June-July-August over 1950–2100 of panel (a) seasonal-mean near-surface relative humidity and (b) the dynamic contribution to changes in precipitation extremes. Results are shown for the 12 models that archived RH_{2m} and for which the dynamic contribution was calculated. Stippling indicates where 10 out the 12 models agree on the sign of the sensitivity. Panel (c) shows a scatter plot of the median sensitivities across land grid boxes in the latitude band 40–70°N for each model.

over land, but these changes are not as well correlated with the dynamic contribution and may be caused by the changes in vertical velocity (Figures S15 and S16 in Supporting Information S1).

The relationship between changes in mean relative humidity and the negative dynamic contribution to changes in extreme precipitation in JJA (Figure 3) is notable in that it links changes in a mean quantity to changes in an extreme statistic. Such a link is potentially very useful since mean quantities can be easier to observationally constrain than extremes. The decrease in relative humidity occurs only over land, and factors such as the changes in moist static stability discussed earlier (Li & O'Gorman, 2020; Tandon et al., 2018), a general weakening of the extratropical storm track in NH JJA (Gertler & O'Gorman, 2019; O'Gorman, 2010), or the poleward expansion of the Hadley cells in the subtropics (Norris et al., 2020; Pfahl et al., 2017) may also influence the dynamic contribution over land and ocean.

In NH DJF, there is not a connection between changes in RH_{2m} and the dynamic contribution (Figure S17 in Supporting Information S1), which we hypothesize is because daily precipitation extremes in DJF are controlled to a greater extent by large-scale dynamics as compared to the strongly convective extremes in JJA.

Interestingly, there is also a negative dynamic contribution over the Southern Hemisphere over both land and ocean in JJA (Figure 1c). This negative dynamic contribution does not show as clear a land-ocean contrast and primarily occurs at lower latitudes as compared to the negative dynamic contribution in the NH, and thus we hypothesize it may be more strongly influenced by factors such as Hadley cell expansion (Norris et al., 2020; Pfahl et al., 2017).

5. Observed and Modeled Trends Over the Historical Period

Given the difficulty in correctly representing convection in models, we next turn our attention to gridded observations of precipitation extremes. Figure 4 shows the sensitivity of daily precipitation extremes from HadEX3 observations and CMIP5 models to warming over 1950–2017 for boreal summer (MJJAS) and extended winter (NDJFM), and the seasonal contrast (MJJAS-NDJFM). The results are expressed as medians for each 5° latitude bands (see Section 2). For the NH extratropics, the observed sensitivities are positive in both MJJAS and NDJFM, and there is a clear summer-winter contrast with lower sensitivities in MJJAS than NDJFM (Figures 4a–4c). The
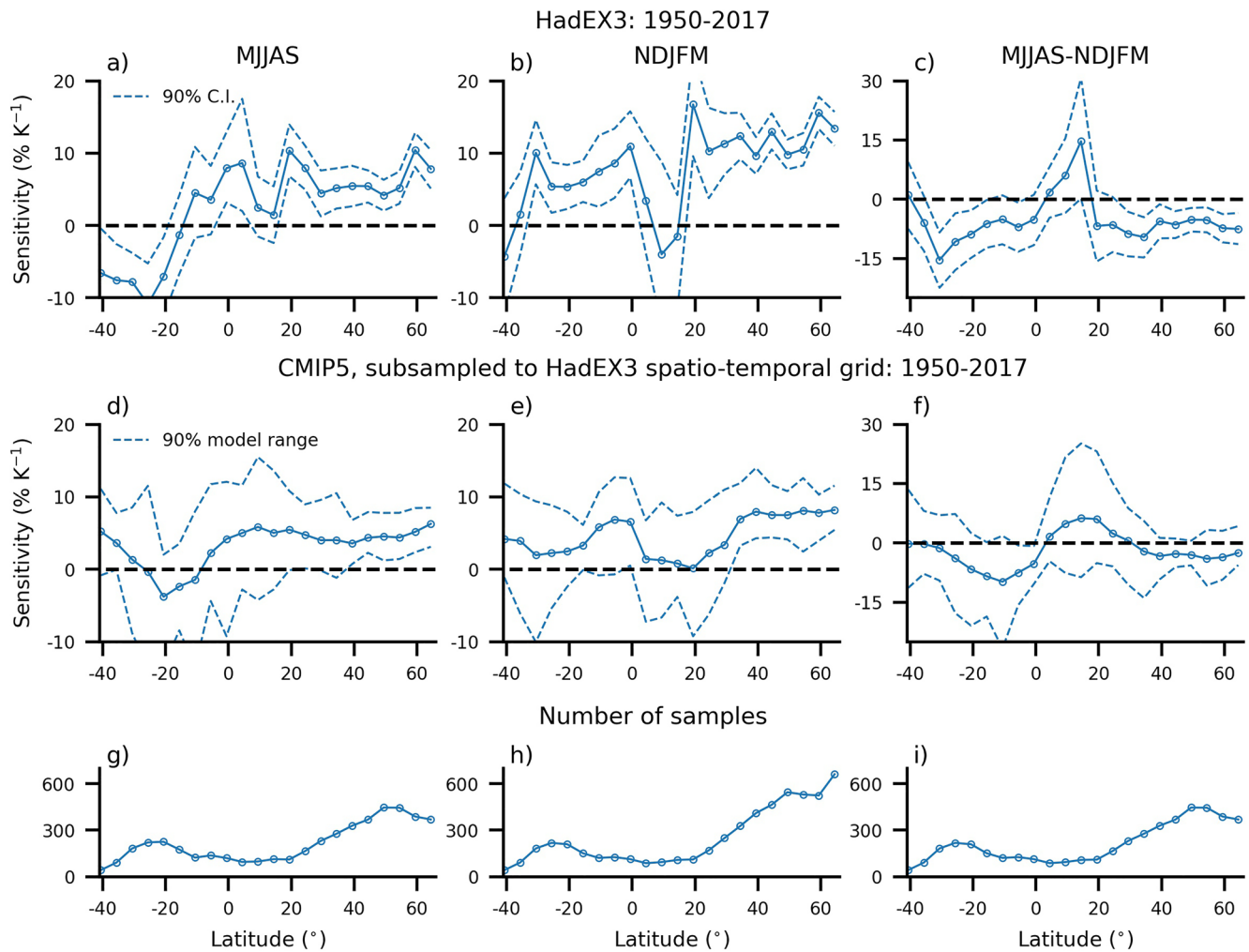
Figure 4. The sensitivity of Rx1day to warming over 1950–2017 in (a and d) MJJAS, (b and e) NDJFM and (c and f) MJJAS-NDJFM for the HadEX3 data set (a,b, and c) and CMIP5 simulations subsampled to the HadEX3 data set (d,e, and f). Solid lines show the median sensitivity across the 5° latitude band. Dashed lines show the 90% confidence interval for HadEX3 and 90% of the model spread for CMIP5. The total number of samples included in each latitude band is also shown (g,h, and i) which is the same for both the observations and the simulations.

seasonal contrast is also evident when looking at maps of the sensitivities, but as expected there is considerable noise when considering sensitivities for a period of this length in individual gridboxes (Figures S18a–S18c in Supporting Information S1). The NH extratropical summer-winter contrast is also present in the CMIP5 models over the same historical period (Figures 4d–4f).

We next quantify the NH midlatitude response by averaging the sensitivities over land between 30 and 70°N with area-weighting. For the observations, the mean NH sensitivity is 5.6% K^{-1} for MJJAS, 11.6% K^{-1} for NDJFM, and -7.2% K^{-1} for MJJAS-NDJFM. For the CMIP5 models over the same period, the multimodel-mean sensitivity and full model range are 4.4% K^{-1} (2.1%–9.1% K^{-1}) for MJJAS, 7.0% K^{-1} (4.7%–10.8% K^{-1}) for NDJFM, and -2.4% K^{-1} (0.6% to -8.4% K^{-1}) for MJJAS-NDJFM. Thus, while the models and observations show similar sensitivities during MJJAS, none of the models capture the very strong observed sensitivity for NDJFM. As a result, while the observed MJJAS-NDJFM contrast lies within the model range, the multi model-mean value is smaller in magnitude than the value in observations. The smaller magnitude of the sensitivity in the multimodel mean than in observations may be related to unforced internal variability, which is reduced by considering the multimodel mean but is likely to be still important in observations. Despite this, most but not all models (15/18) give a negative MJJAS-NDJFM contrast for this period, consistent with the observations.

GHCNDEX has a coarser spatial resolution and fewer grid boxes with data compared to HadEX3, particularly in the tropics, but we find similar changes in seasonal Rx1day over the NH (Figures S18 and S19 in Supporting Information S1), which strengthens our confidence in the results. Similar results are also found when the CMIP5 data are not subsampled to the observations (Figure S20 in Supporting Information S1), which suggests that missing grid points in the observations are not affecting our conclusions. The robust presence of the MJJAS-NDJFM contrast in observed trends over the historical period supports the contrast found in earlier sections.

6. Conclusions

In this study we have demonstrated that CMIP5 models project a robust summer-winter contrast in the response of precipitation extremes to warming over NH midlatitude land, with considerably weaker percentage changes in JJA than DJF. We have also shown that this summer-winter contrast is evident in gridded observations over the historical period, which strengthens our confidence in the future projections. CMIP5 simulations over the historical period also show a summer-winter contrast that occurs in 15/18 models, and the model range includes the observed value of this contrast.

Furthermore, we have used a simple, physical scaling to help explain the cause of the summer-winter contrast in changes in precipitation extremes. The contrast is primarily caused by the dynamic contribution (related to changes in extreme ascent) with strongly negative dynamic contribution in JJA and a weakly positive dynamic contribution in DJF. The negative dynamic contribution in JJA is strong over NH extratropical land, and we show it is correlated with decreases in near-surface relative humidity in terms of spatial pattern and inter-model scatter. The negative dynamic contribution is also correlated with increases in seasonal CIN but less so for CIN on the day of the extreme precipitation event, and thus further work is required to investigate the dynamical mechanism involved and demonstrate causality.

The thermodynamic contribution to changes in precipitation extremes also helps to amplify the response in winter over summer, particularly over high latitudes. We have focused on percentage seasonal changes because they may be more relevant for impacts in a given season and to better connect with physical mechanisms. If absolute rather than percentage changes in precipitation extremes are considered, the thermodynamic contribution is larger in summer than winter, and this offsets the JJA-DJF contrast in the dynamic contribution, although the contrast is still evident over much of NH midlatitude land (Figure S5 in Supporting Information S1).

Future work could build on our observational analysis by performing a formal detection and attribution analysis of the seasonal difference in trends of precipitation extremes. Future work could also build more understanding of the positive dynamic contribution in the NH extratropics in winter, which is important as DJF is the season of maximum daily precipitation in many regions (Marelle et al., 2018). Future work could also investigate the detailed mechanism of the link between changes in relative humidity and precipitation extremes in summer using idealized experiments in cloud-resolving models, which would also help to establish the physical reliability of this link. Given the potential importance of decreases in relative humidity over land for convection and precipitation extremes, it would be helpful to develop an emergent constraint for the magnitude of the expected decrease, although this may be difficult to the extent that it depends both on the land-ocean warming contrast and the plant physiological response to increased on CO_2 levels.

Data Availability Statement

Processed observational and climate model data supporting the conclusions in this study can be found at https://doi.org/10.5281/zenodo.6341493.

References

Ban, N., Schmidli, J., & Schär, C. (2015). Heavy precipitation in a changing climate: Does short-term summer precipitation increase faster? *Geophysical Research Letters*, 42(4), 1165–1172. https://doi.org/10.1002/2014GL062588

Berg, A., Findell, K., Lintner, B., Giannini, A., Seneviratne, S. I., van den Hurk, B., et al. (2016). Land–atmosphere feedbacks amplify aridity increase over land under global warming. *Nature Climate Change*, 6(9), 869–874. https://doi.org/10.1038/nclimate3029

Byrne, M. P., & O'Gorman, P. A. (2016). Understanding decreases in land relative humidity with global warming: Conceptual model and GCM simulations. *Journal of Climate*, 29(24), 9045–9061. https://doi.org/10.1175/JCLI-D-16-0351.1

Byrne, M. P., & O'Gorman, P. A. (2018). Trends in continental temperature and humidity directly linked to ocean warming. *Proceedings of the National Academy of Sciences*, *115*(19), 4863–4868. https://doi.org/10.1073/pnas.1722312115

Cao, L., Bala, G., Caldeira, K., Nemani, R., & Ban-Weiss, G. (2010). Importance of carbon dioxide physiological forcing to future climate change. *Proceedings of the National Academy of Sciences*, *107*(21), 9513–9518. https://doi.org/10.1073/pnas.0913000107

Chan, S. C., Kendon, E. J., Fowler, H. J., Blenkinsop, S., Roberts, N. M., & Ferro, C. A. T. (2014). The value of high-resolution met office regional climate models in the simulation of multihourly precipitation extremes. *Journal of Climate*, *27*(16), 6155–6174. https://doi.org/10.1175/JCLI-D-13-00723.1

Chen, J., Dai, A., Zhang, Y., & Rasmussen, K. L. (2020). Changes in convective available potential energy and convective inhibition under global warming. *Journal of Climate*, *33*(6), 2025–2050. https://doi.org/10.1175/JCLI-D-19-0461.1

Diffenbaugh, N. S., & Burke, M. (2019). Global warming has increased global economic inequality. *Proceedings of the National Academy of Sciences*, *116*(20), 9808–9813. https://doi.org/10.1073/pnas.1816020116

Donat, M. G., Alexander, L. V., Yang, H., Durre, I., Vose, R., Dunn, R. J. H., et al. (2013). Updated analyses of temperature and precipitation extreme indices since the beginning of the twentieth century: The HadEX2 dataset. *Journal of Geophysical Research: Atmospheres*, *118*(5), 2098–2118. https://doi.org/10.1002/jgrd.50150

Donat, M. G., Lowry, A. L., Alexander, L. V., O'Gorman, P. A., & Maher, N. (2016). More extreme precipitation in the world's dry and wet regions. *Nature Climate Change*, *6*(5), 508–513. https://doi.org/10.1038/nclimate2941

Dunn, R. J. H., Alexander, L. V., Donat, M. G., Zhang, X., Bador, M., Herold, N., et al. (2020). Development of an updated global land in situ-based data set of temperature and precipitation extremes: HadEX3. *Journal of Geophysical Research: Atmospheres*, *125*(16), e2019JD032263. https://doi.org/10.1029/2019JD032263

Fischer, E. M., Sedláček, J., Hawkins, E., & Knutti, R. (2014). Models agree on forced response pattern of precipitation and temperature extremes. *Geophysical Research Letters*, *41*(23), 8554–8562. https://doi.org/10.1002/2014GL062018

Gertler, C. G., & O'Gorman, P. A. (2019). Changing available energy for extratropical cyclones and associated convection in Northern Hemisphere summer. *Proceedings of the National Academy of Sciences*, *116*(10), 4105–4110. https://doi.org/10.1073/pnas.1812312116

Kharin, V. V., Zwiers, F. W., Zhang, X., & Wehner, M. (2013). Changes in temperature and precipitation extremes in the CMIP5 ensemble. *Climatic Change*, *119*(2), 345–357. https://doi.org/10.1007/s10584-013-0705-8

Kirschbaum, D., Adler, R., Adler, D., Peters-Lidard, C., & Huffman, G. (2012). Global distribution of extreme precipitation and high-impact landslides in 2010 relative to previous years. *Journal of Hydrometeorology*, *13*(5), 1536–1551. https://doi.org/10.1175/JHM-D-12-02.1

Knapp, A. K., Beier, C., Briske, D. D., Classen, A. T., Luo, Y., Reichstein, M., et al. (2008). Consequences of more extreme precipitation regimes for terrestrial ecosystems. *BioScience*, *58*(9), 811–821. https://doi.org/10.1641/b580908

Kooperman, G. J., Pritchard, M. S., & Somerville, R. C. J. (2014). The response of US summer rainfall to quadrupled CO_2 climate change in conventional and superparameterized versions of the NCAR community atmosphere model. *Journal of Advances in Modeling Earth Systems*, *6*(3), 859–882. https://doi.org/10.1002/2014MS000306

Lepore, C., Allen, J., & Abernathey, R. (2021). *xcape*. Zenodo. https://doi.org/10.5281/zenodo.5270332

Li, Z., & O'Gorman, P. A. (2020). Response of vertical velocities in extratropical precipitation extremes to climate change. *Journal of Climate*, *33*(16), 7125–7139. https://doi.org/10.1175/JCLI-D-19-0766.1

Marelle, L., Myhre, G., Hodnebrog, i., Sillmann, J., & Samset, B. H. (2018). The changing seasonality of extreme daily precipitation. *Geophysical Research Letters*, *45*(20), 11352–11360. https://doi.org/10.1029/2018GL079567

Muller, C. J., O'Gorman, P. A., & Back, L. E. (2011). Intensification of precipitation extremes with warming in a cloud-resolving model. *Journal of Climate*, *24*(11), 2784–2800. https://doi.org/10.1175/2011JCLI3876.1

Norris, J., Chen, G., & Li, C. (2020). Dynamic amplification of subtropical extreme precipitation in a warming climate. *Geophysical Research Letters*, *47*(14), e2020GL087200. https://doi.org/10.1029/2020GL087200

O'Gorman, P. A. (2010). Understanding the varied response of the extratropical storm tracks to climate change. *Proceedings of the National Academy of Sciences*, *107*(45), 19176–19180. https://doi.org/10.1073/pnas.1011547107

O'Gorman, P. A. (2015). Precipitation extremes under climate change. *Current Climate Change Reports*, *1*(2), 49–59. https://doi.org/10.1007/s40641-015-0009-3

O'Gorman, P. A., Li, Z., Boos, W. R., & Yuval, J. (2021). Response of extreme precipitation to uniform surface warming in quasi-global aqua-planet simulations at high resolution. *Philosophical Transactions of the Royal Society A: Mathematical, Physical & Engineering Sciences*, *379*(2195), 20190543. https://doi.org/10.1098/rsta.2019.0543

O'Gorman, P. A., & Schneider, T. (2009a). The physical basis for increases in precipitation extremes in simulations of 21st-century climate change. *Proceedings of the National Academy of Sciences*, *106*(35), 14773–14777. https://doi.org/10.1073/pnas.0907610106

O'Gorman, P. A., & Schneider, T. (2009b). Scaling of precipitation extremes over a wide range of climates simulated with an idealized gcm. *Journal of Climate*, *22*(21), 5676–5685. https://doi.org/10.1175/2009JCLI2701.1

Pfahl, S., O'Gorman, P. A., & Fischer, E. M. (2017). Understanding the regional pattern of projected future changes in extreme precipitation. *Nature Climate Change*, *7*(6), 423–427. https://doi.org/10.1038/nclimate3287

Pichelli, E., Coppola, E., Sobolowski, S., Ban, N., Giorgi, F., Stocchi, P., et al. (2021). The first multi-model ensemble of regional climate simulations at kilometer-scale resolution Part 2: Historical and future simulations of precipitation. *Climate Dynamics*, *56*(11), 3581–3602. https://doi.org/10.1007/s00382-021-05657-4

Prein, A. F., Langhans, W., Fosser, G., Ferrone, A., Ban, N., Goergen, K., et al. (2015). A review on regional convection-permitting climate modeling: Demonstrations, prospects, and challenges. *Reviews of Geophysics*, *53*(2), 323–361. https://doi.org/10.1002/2014RG000475

Prein, A. F., Rasmussen, R. M., Ikeda, K., Liu, C., Clark, M. P., & Holland, G. J. (2017). The future intensification of hourly precipitation extremes. *Nature Climate Change*, *7*(1), 48–52. https://doi.org/10.1038/nclimate3168

Singh, M. S., & O'Gorman, P. A. (2013). Influence of entrainment on the thermal stratification in simulations of radiative-convective equilibrium. *Geophysical Research Letters*, *40*(16), 4398–4403. https://doi.org/10.1002/grl.50796

Sippel, S., Zscheischler, J., Heimann, M., Lange, H., Mahecha, M. D., van Oldenborgh, G. J., et al. (2017). Have precipitation extremes and annual totals been increasing in the world's dry regions over the last 60 years? *Hydrology and Earth System Sciences*, *21*(1), 441–458. https://doi.org/10.5194/hess-21-441-2017

Tandon, N. F., Nie, J., & Zhang, X. (2018). Strong influence of eddy length on boreal summertime extreme precipitation projections. *Geophysical Research Letters*, *45*(19), 10665–10672. https://doi.org/10.1029/2018GL079327

Taylor, K. E., Stouffer, R. J., & Meehl, G. A. (2012). An overview of CMIP5 and the experiment design. *Bulletin of the American Meteorological Society*, *93*(4), 485–498. https://doi.org/10.1175/BAMS-D-11-00094.1

Vose, R. S., Arndt, D., Banzon, V. F., Easterling, D. R., Gleason, B., Huang, B., et al. (2012). NOAA's merged land–ocean surface temperature analysis. *Bulletin of the American Meteorological Society*, *93*(11), 1677–1685. https://doi.org/10.1175/BAMS-D-11-00241.1

Wehner, M., Gleckler, P., & Lee, J. (2020). Characterization of long period return values of extreme daily temperature and precipitation in the CMIP6 models: Part 1, model evaluation. *Weather and Climate Extremes*, *30*, 100283. https://doi.org/10.1016/j.wace.2020.100283

Wood, R. R., & Ludwig, R. (2020). Analyzing internal variability and forced response of subdaily and daily extreme precipitation over Europe. *Geophysical Research Letters*, *47*(17), e2020GL089300. https://doi.org/10.1029/2020GL089300